CONTROLLED MOTION OF A CYLINDER THROUGH A FREE SURFACE: EFFECT OF DEPTH OF PENETRATION

J.-C. Lin, N. Phetkong, J. Sheridan and D. Rockwell
*Department of Mechanical Engineering and Mechanics, Lehigh University
Bethlehem, Pennsylvania 18015, U.S.A.*

A cylinder undergoing vertical oscillation penetrates a free surface. The oscillation is controlled to maintain constant maximum acceleration for a range of values of penetration depth. High-image-density particle image velocimetry, which provides instantaneous representations of the vortex development, reveals that several patterns of nearly symmetrical vortices can occur during an oscillation cycle. They originate from distinctive mechanisms of flow separation and vorticity layer development. The key role of the penetration process through the free surface is emphasized by comparison with the corresponding case of the completely submerged cylinder, which generates highly asymmetrical patterns of vortices. An important common feature, however, is the initial formation of a counterflow mixing-layer, corresponding to an elongated layer of vorticity, from the surface of the cylinder. This layer exhibits small-scale Kelvin-Helmholtz vortices and eventually comprises a large-scale vortex.

© 1996 Academic Press Limited

1. INTRODUCTION

THE UNSTEADY FLOW PATTERNS arising from oscillation of a completely submerged cylinder in a quiescent fluid, or oscillatory flow past a stationary cylinder, have been of considerable interest over the past two decades. When the amplitude of the oscillation is sufficiently large, vortices are shed from the cylinder during the oscillation cycle, giving rise to complex patterns of them, which, in turn, are linked to both drag and lift components of loading on the cylinder. A wide variety of modes of vortex formation may occur; they are principally dependent upon the value of the dimensionless amplitude $KC \equiv 2\pi A/D$, known as the Keulegan-Carpenter number. The many interesting features of these patterns and the associated loading on the cylinder are described by Maull & Milliner (1978), Singh (1979), Sarpkaya & Isaacson (1981), Iwagaki, Asano & Nagai (1983), Williamson (1985), Bearman, Downie, Graham & Obasaju (1985), and Obasaju, Bearman & Graham (1988).

In contrast to all of the foregoing investigations, the present study addresses the case of an oscillating cylinder that does not remain submerged during the entire cycle. Rather, a portion of the oscillation cycle is in air and the remainder in water, such that the penetration process through the free surface and the history of the cylinder motion while it is submerged play a key role in determining the patterns and strengths of vortical structures formed from the cylinder. In a practical sense, this configuration has relevance to wave "slamming" and, more generally, to free-surface waves translating past a suspended cylinder. From a fundamental standpoint, however, this study is expected to provide insight into the process of unsteady vortex formation due to an abrupt change in fluid medium during the oscillation cycle. An understanding of the manner in which the vorticity layer is formed from the cylinder and gives rise to

large-scale concentrations of vorticity, in relation to the corresponding case of the completely submerged oscillating cylinder, is a primary objective of the present investigation. High-image-density particle image velocimetry is employed to determine the instantaneous flow structure in terms of velocity, vorticity and streamlines.

2. EXPERIMENTAL SYSTEM AND TECHNIQUES

Experiments were performed in a free-surface test section having a width of 210 mm and a depth of 527 mm. A cylinder of diameter $D = 25 \cdot 4$ mm was mounted horizontally at a defined equilibrium position beneath the free surface, as indicated in the schematic of Figure 1. The cylinder was held in position by a vertical arm, which was located on the opposite side of a false wall arrangement, thereby ensuring that the presence of the arm did not influence the unsteady flow field past the cylinder. Oscillations of the cylinder were controlled by a high resolution Compumotor, controlled by a central microcomputer. The amplitude of the oscillation was $A = 40$ mm, corresponding to a dimensionless amplitude $A^* \equiv A/D = 1 \cdot 57$. The frequency, f, of the oscillation was kept constant at $0 \cdot 33$ Hz, corresponding to a value of the dimensionless frequency parameter $\beta = fD^2/\nu = 227$. Values of the equilibrium position $h = 26 \cdot 7$, $6 \cdot 7$, and $-13 \cdot 3$ mm corresponded to dimensionless values of $h^* = h/D = 1 \cdot 1$, $0 \cdot 3$, and $-0 \cdot 5$. Since the amplitude, A^*, and frequency, $\omega = 2\pi f$, of the cylinder oscillation were maintained constant, the maximum acceleration, $A\omega^2$, of the cylinder was likewise constant at a value of 175 mm/s^2, allowing examination of the effect of equilibrium position h^* on the process of vortex formation. As indicated in Figure 1, the instantaneous position of the cylinder is defined by distance η beneath the free-surface, or in dimensionless form, $\eta^* = \eta/D$. For purposes of comparison, the case of the completely submerged cylinder was also investigated. In this case, the amplitude, A, and frequency, f, of the cylinder oscillation beneath the free-surface oscillation were the same as in the foregoing, but the nominal position of the cylinder was well below the surface at a distance $h^* = 4 \cdot 3$.

Instantaneous images of the flow structure were obtained using a scanning-laser version of high-image-density particle image velocimetry described by Rockwell,
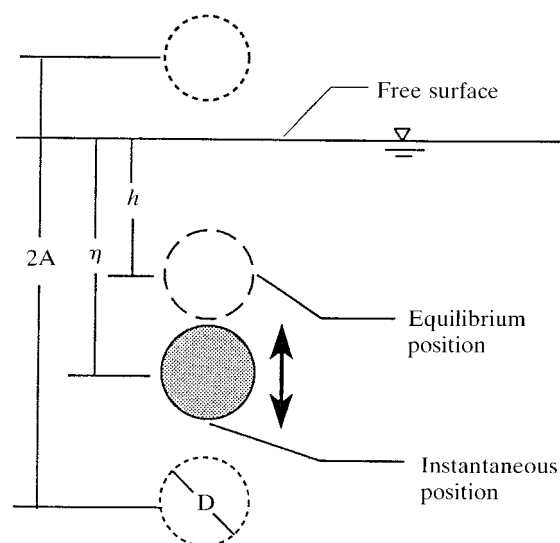
Figure 1. Overview of experimental arrangement and definition of parameters.

Magness, Towfighi, Akin & Corcoran (1993). The water was seeded with 12μ diameter, metallic-coated particles. Multiply exposed images of each particle were generated by rapidly scanning the beam of a 20 W Argon-ion laser over the plane of interest. This scanning laser sheet was produced by reflecting the beam from a rotating mirror having 72 facets. The effective scanning frequency, generated by this approach, was 626 Hz. Images were recorded on 35 mm film having a high resolution of 300 lines per mm. These images were then digitized and interrogated using a single-frame cross-correlation technique. The dimensions of the interrogation window were 90 pixels $\times$ 90 pixels, corresponding to 0·72 mm $\times$ 0·72 mm. The magnification of the camera lens was 1:4, providing an effective grid dimension in the plane of the laser sheet of 2·88 mm.

3. OVERVIEW OF FLOW STRUCTURE DURING OSCILLATION CYCLE

The three successive layouts of vorticity and velocity fields of Figures 2(a) through 2(c) show selected excerpts of the evolving flow structure from the cylinder, first during the upstroke, then the downstroke motion of the cylinder. In Figure 2(a), the instantaneous position of the cylinder is designated by phase angle ϕ; $\phi = 0$ corresponds to the maximum depth of penetration of the cylinder. This layout of images exhibits two pairs of vortical structures: A-B and C-D. Pair A-B arises from vortex generation during the early part of the downstroke motion, immediately after penetration of the free surface. Pair C-D arises near the maximum depth of penetration at $\phi = 0°$. As indicated in the velocity distribution at $\phi = 8°$, shortly after attainment of maximum submergence at ($\phi = 0°$), all vorticity concentrations are thrust outward with a relatively large velocity.

   During a later stage of the upstroke motion, represented by $\phi = 32°$ in Figure 2(a), the vorticity concentrations A and B form pairs with vortices C and D, i.e. A-C and B-D. This process continues to involve relatively large velocity.

   During a later stage of the upstroke motion, represented by $\phi = 32°$ in Figure 2(a), the vorticity concentrations A and B form pairs with vortices C and D, i.e. A-C and B-D. This process continues to involve relatively large velocities, directed away from the cylinder at an angle of about 45° to its line of motion. At the next instant during the upstroke, represented by $\phi = 56°$, vorticity concentrations A and B move further downward, as do concentrations C and D, the latter remaining connected to the surface of the cylinder through a layer of vorticity.

   Further development of the wake of the cylinder is shown in Figure 2(b). At $\phi = 80°$, vorticity concentrations A through C have a distinct identity and lie approximately at the same horizontal level. As indicated in the corresponding image of the velocity field, this system of vortices is moving rapidly downward. At later instants, vorticity is continuously shed from the cylinder, and extended vorticity layers are evident at $\phi = 104°$. No pronounced, large-scale concentrations of vorticity have developed. At $\phi = 128°$, however, the regions of positive and negative vorticity detach entirely from the submerged surface of the cylinder. This rapid detachment process is driven by penetration of the cylinder through the free surface. During detachment, each of the vorticity layers agglomerates into a large-scale concentration of vorticity.

   The final phase of development of the wake is shown in Figure 2(c). At $\phi = 152°$, the elliptically shaped vorticity contours are abruptly reoriented, such that their major axis is oriented parallel to the free surface. At a later instant, corresponding to $\phi = 176°$, the concentrations E and F eventually induce, through interaction with the free surface, counter-concentrations G and H. Even at this relatively late stage of the cylinder-free surface interaction, the concentrations of vorticity move outward at a relatively high velocity. In fact, the patterns of vectors at $\phi = 224°$, corresponding to re-penetration of

the cylinder through the free surface, show large magnitudes of velocity parallel to the free surface at locations well away from the region of penetration.

All of the foregoing events occur over a relatively short time span, emphasizing that small changes in the instantaneous elevation of the cylinder with respect to the free surface produce large changes in the form and orientation of the vorticity concentrations. Inspection of the corresponding velocity distributions at $\phi = 128°$ and $152°$ shows that these changes of the vorticity distributions are accompanied by large velocities arising from interaction of the cylinder with the free surface.

4. PHASE-REFERENCED PATTERNS OF FLOW STRUCTURE

In order to compare the patterns of flow structure at different equilibrium positions of the cylinder $h^* = h/A$, it is insightful to examine images at the same phase of the oscillation cycle, while the amplitude A^* of the cylinder motion is maintained constant. For a given value of phase ϕ, the displacement, velocity and acceleration of the cylinder will therefore be the same, even though the equilibrium position h^* and therefore the maximum depth of penetration are different. Phase angle $\phi = 0°$ corresponds to the maximum penetration of the cylinder during the downstroke. Instantaneous vorticity and velocity distributions corresponding to three values of phase angle $\phi = 32°$, $56°$, and $80°$ are shown in Figures 3(a) through 3(c).

In Figure 3(a), at the deepest equilibrium position, $h^* = 1·1$, vortices A through D all have a relatively large value of dimensionless circulation $\Gamma^* = \Gamma/\pi U_m D$ lying in the range $-0·54 \leq \Gamma^* \leq 0·57$. When h^* is decreased to $0·3$, the general pattern of the vorticity concentrations A through D remains essentially the same. The typical values of circulation are, however, decreased significantly; they lie in the range $-0·24 \leq \Gamma^* \leq 0·18$, with vortices A and B having values of $\Gamma^* = -0·24$ and $0·18$. Finally, at the smallest value of $h^* = -0·5$, corresponding to a position just above the free surface, significant concentrations of vorticity are not formed. Now, according to Figure 1, the distance that the center of the cylinder remains beneath the free surface is $A^* + h^*$. For values of $h^* = 1·1$, $0·3$, and $-0·5$ shown in Figure 3(a), the corresponding values of $A^* + h^* = 2·7$, $1·9$ and $1·1$. There appears to be a threshold value of $A^* + h^*$, below which vortices A and B are not formed, and therefore vortices C and D are not induced. The images at $h^* = -0·5$ clearly correspond to a value of $A^* + h^*$ below the threshold. Furthermore, for cases $h^* = 1·1$ and $0·3$, which clearly lie above this threshold, the circulation Γ^* of vortices A and B decreases with decreasing values of $A^* + h^*$, and thereby the circulation of vortices C and D correspondingly decreases.

Figure 3(b) shows the flow structure at the phase angle $\phi = 56°$. At the deepest equilibrium position $h^* = 1·1$, vortices A and B are completely detached from the cylinder, whereas C and D are connected to the cylinder surface by an elongated layer of vorticity. These identifiable concentrations C and D are substantially distorted, relative to their counterparts at $\phi = 32°$, by the complex, induced velocity field about the bottom surface of the cylinder. Similar patterns of vorticity and velocity are shown at the intermediate penetration depth $h^* = 0·3$. At $h^* = -0·5$, however, significant vorticity concentrations are not evident, as already suggested at $\phi = 32°$ in Figure 3(a).

Figure 3(c) shows the next stage of evolution, corresponding to $\phi = 80°$. At the maximum and intermediate equilibrium positions $h^* = 1·1$ and $0·3$, identifiable concentrations of vorticity C and D are nearly or completely detached from the continuous layer of vorticity extending from the surface of the cylinder. The vortex systsem A through D tends to lie along the same horizontal elevation. A further interesting feature is that the vorticity layers extending from the bottom surface of the

cylinder tend to merge together at $h^* = 1.1$ and 0.3. This tendency towards merging is due to the highly distorted velocity field induced by the cylinder-free surface interaction. As is particularly evident in the velocity image at $h^* = 1.1$, pronounced downward flow along the sides of the cylinder occurs simultaneously with upward flow along the plane of the symmetry of the cylinder wake. In fact, this velocity field can be viewed as a system of two counterflow mixing layers, corresponding to the elongated layers of vorticity, with embedded small-scale concentrations arising from the Kelvin-Helmholtz instabilities.

5. SURFACE-REFERENCED PATTERNS OF FLOW STRUCTURE

Figure 4(a) shows comparisons of the vorticity distributions and velocity fields for the same instantaneous position of the cylinder relative to the free surface as a function of equilibrium position h^*.

For both $h^* = 1.1$ and -0.1, the elevation of the free surface is maximum at the cylinder-surface junction and exhibits a minimum, i.e. a trough, at a distance of about $1D$ from the junction. The velocity field in the left column of Figure 4(a), corresponding to $h^* = 1.1$, exhibits large variations in the vertical component of the velocity just beneath the free surface at increasing distance from the center of the cylinder. Immediately adjacent to the cylinder, the large positive (upward) component is bounded by a strong downward component. These drastic variations of magnitude and direction of vertical velocity are directly related to the concentrations of vorticity in those regions.

The images shown in the right column of Figure 4(a) correspond to the value of penetration depth $h^* = -0.1$. For this case, the velocity immediately beneath the free surface, in the region adjacent to the cylinder, does not exhibit the large changes in magnitude and sign apparent for the case $h^* = 1.1$. Moreover, large-scale swirl regions of velocity vectors are not detectable in the region beneath the surface of the cylinder. These observations suggest generally weaker concentrations of vorticity, corroborated by the corresponding vorticity distributions; they take the form of vorticity layers in close proximity to the surface of the cylinder and exhibiting small-scale concentrations characteristic of a Kelvin-Helmholtz instability.

Corresponding streamline patterns are given in the bottom row of Figure 4(a). For the image at $h^* = 1.1$, the streamlines show the intimate relationship between the vorticity concentrations near the free surface-cylinder junction and the upward flow along the center of the wake induced by the motion of the cylinder. At $h^* = -0.1$, on the other hand, swirling streamline patterns do not exist, due to the lack of the large-scale concentrations of vorticity. In fact, on the basis of this streamline pattern, it is not possible to deduce existence of the layers of vorticity, which are essentially distributed, but possess a substantial value of circulation.

Further development of the streamline pattern at $h^* = 1.1$ is shown in Figure 4(b). Vorticity concentrations E and F are now associated with limit cycles, i.e, closed streamlines; outside of these cycles, the streamlines spiral outward, and inside of them they spiral inward, meaning that the limit cycles are unstable.

6. COMPARISON OF PATTERNS OF FLOW STRUCTURE FROM SURFACE-PIERCING AND COMPLETELY SUBMERGED CYLINDER

In order to emphasize the distinction between the patterns of vorticity from a completely submerged oscillating cylinder and the foregoing cases of the surface-piercing cylinder, the cylinder was lowered to a nominal depth of $h^* = 4.3$ and

subjected to the same dimensionless amplitude of oscillation $A^* = 1 \cdot 57$ as for the oscillating cylinder, corresponding to a value of the Keulegan-Carpenter $KC = 9 \cdot 89$. Comparison of the instantaneous flow structure at the same value of phase angle, ϕ, for both the surface-piercing and submerged cylinders is given in Figures 5(a) and 5(b). As in the foregoing cases, the phase angle $\phi = 0°$ corresponds to the maximum depth of penetration, i.e., the extreme displacement of the cylinder during the downstroke motion. For the case of the completely submerged cylinder, the patterns of vortex formation are highly asymmetrical and correspond to formation of one vortex during each half-cycle of the cylinder oscillation. These observations are in general accordance with those of Williamson (1985) and Obasaju et al. (1988). At $\phi = 80°$, vortex B is fully formed and detached from the cylinder. The region of vorticity A is linked to the surface of the cylinder. At $\phi = 104°$, the large-scale concentration A is about to detach from the surface of the cylinder. Finally, at $\phi = 152°$, concentration of vorticity C is about to detach from the lower surface of the cylinder. This process of highly asymmetrical vortex formation involves separation of a curved vorticity layer from the bottom surface of the cylinder; this layer is actually composed of several discrete concentrations of vorticity, due to the Kelvin-Helmholtz instability.

Figure 5(b) shows the corresponding velocity distributions and streamline patterns for the fully submerged cylinder. The instantaneous velocity field shows that the separation process gives rise to a mixing-layer configuration wrapped around the bottom surface of the cylinder. It is the rollup of this layer that is associated with the eventual formation of the vorticity concentration C in Figure 5(a). This process of vortex formation is in marked contrast to the corresponding scenario for the surface-piercing cylinder shown at the same values of phase angle in Figures 2(b) and 2(c). Recall that it involves formation of an elongated layer of vorticity between two counter-flow streams, which is eventually clipped due to the piercing process with the free surface. This clipping of the free surface appears to be central to the rapid concentration of vorticity into defined vortical structures. Such a clipping process does not occur for the completely submerged case.

The corresponding distributions of streamline patterns of Figure 5(b) show the general features of the vorticity concentrations of Figure 5(a). These streamlines represent the integrated velocity field and therefore drastically smooth out the actual, smaller-scale concentrations of vorticity which comprise the large-scale swirl regions. This smoothing is particularly evident for the region of vorticity designated as vortex A. Such streamline patterns are representative of the particle-streak images typically employed in investigations of oscillating cylinders.

7. CLASSIFICATION OF NEAR-WAKE PATTERNS LEADING TO VORTEX FORMATION

An overview of the basic types of velocity fields in the very near-wake of the cylinder is given in Figure 6. Each of these patterns is associated with a particular type of vorticity layer development, eventually leading to formation of discrete vortices, in the manner described in the foregoing. For the case of the surface-piercing cylinder, represented by images (a) through (c), the gross separation patterns are essentially symmetrical with respect to the plane of symmetry of the wake. The distinguishing feature of the pattern of (a) is that a pre-existing vortex system, designated as vortices A and B in Figure 2(a) (at $\phi = 32°$) induces the jet-like flow at an angle of approximately 45° on the left and right sides of the cylinder. This jet-like flow having relatively high velocity leads to eruption of the boundary layer from the surface of the cylinder and to formation of

vortices C and D (compare Figure 2(a), $\phi = 32°$). This formation of secondary vortices C and D occurs in accordance with the mechanism originally described by Walker (1978) and addressed in a range of subsequent studies assessed by Doligalski, Smith & Walker (1994). The process of boundary-layer separation leading to formation of the secondary vortices appears to take the form of a sharply focused eruption of the boundary layer from the surface of the cylinder, as described for other types of vortex-boundary layer interaction by Doligalski *et al.* (1994).

On the other hand, for the types of patterns shown in images (b) and (c) in Figure 6, there are no pre-existing vortices of the type A and B occurring in image (a). Rather, in these cases, the downflow along the sides of the cylinder coexists with a column of fluid moving in the upward direction through the center of the cylinder wake, giving rise to two counter-flow mixing layers, corresponding to extended vorticity layers from the surface of the cylinder (compare Figure 3(c), $h* = 1·1$ and $0·3$). This configuration appears to be a central feature of all of the foregoing cases of the surface-piercing cylinder as it approaches the free-surface; it seems to preclude roll-up of the vorticity layers into large-scale vorticity concentrations. To be sure, these vorticity layers do exhibit small-scale concentrations of vorticity arising from the Kelvin–Helmholtz instability, as evident, for example, in Figure 3(c). Only when they are clipped away from the surface of the cylinder by actual penetration through the surface do large-scale vortical structures become apparent; compare Figure 2(b), $\phi = 128°$.

This configuration of the counterflow mixing layer also exists for the case of the completely submerged cylinder shown in image (d) of Figure 6. In this case, however, there is only one such layer, in contrast to the pairs of layers in images (b) and (c) for the surface-piercing cylinder. When the cylinder is completely submerged, strong asymmetry of the wake sets in, due to sweeping of flow around the entire base of the cylinder, such that an upward flow exists on the right-hand side, opposing the downward flow and forming a counter-flow mixing-layer. Correspondingly, a layer of vorticity is generated, with embedded, small-scale concentrations of vorticity arising from the Kelvin-Helmholtz instability (compare Figure 5(a), $\phi = 104°$). Unlike the case of the surface-piercing cylinder, where the piercing process allows agglomeration of vorticity into a large-scale structure, the type of asymmetrical pattern shown in Figure 6 for the completely submerged cylinder leads to large-scale vortex formation in the absence of any surface-piercing effects.

8. CONCLUDING REMARKS

Vortex formation and development from an oscillating cylinder penetrating a free surface is strongly influenced by the penetration process, not only during penetration, but also at much later times when the cylinder is well submerged beneath the surface. In other words, there is a history effect that appears to persist over the entire oscillation cycle. The most obvious consequence is a remarkable tendency towards symmetry of the patterns of vortices, which differ from the highly asymmetrical patterns formed from the completely submerged cylinder having the same maximum value of acceleration.

Irrespective of the maximum depth of penetration of the cylinder, the patterns of vortices are similar at a given phase angle of the cylinder displacement. The circulation of these vortices is, however, a strong function of the depth of penetration. In fact, at sufficiently small penetration depth, no vortices are formed; this limit is analogous to the potential flow limit at low values of Keulegan-Carpenter number, KC, for a fully submerged oscillating cylinder.

The remarkable symmetry of the vortex patterns during an oscillation cycle is due to two primary effects: symmetry of the shed vorticity immediately following penetration of the free surface during both the down- and upstroke motion of the cylinder; and rapid convection of shed vortices in an outward direction along the free surface. This preservation of symmetry of the vortex patterns contrasts with the well-known case of the fully submerged cylinder, which exhibits highly asymmetrical vortex formation at sufficiently large values of KC when shed vortices are swept back to the opposite side of the cylinder during an oscillation cycle.

Two distinctive mechanisms of vortex formation can occur after the cylinder has penetrated the free surface. The first involves, in an initial stage, formation of a pair of vortices during the downstroke motion in the traditional manner of vortex formation from an impulsively started cylinder. Then, near the maximum depth of penetration, this system of two vortices induces rapid boundary-layer separation from the surface of the cylinder, giving rise to secondary vortices of opposite sense, which quickly attain a value of circulation commensurate with that of the initially formed vortex system. This process of formation of the secondary vortices involves a highly focused separation from the surface of the cylinder, which is driven by each of the pre-existing vortices formed during the initial phase of the downstroke. The second type of vortex formation occurs during the upstroke motion of the cylinder. An elongated layer of vorticity is formed from the surface of the cylinder, which is compatible with the existence of a mixing-layer-type flow between two counterflowing streams. The downward-oriented stream arises from the induced flow along the sides of the cylinder, which is enhanced as the cylinder approaches the free surface. The upward-oriented stream in the central portion of the wake is induced by the upward motion of the base of the cylinder. Although small-scale Kelvin-Helmholtz instabilities are evident in the elongated layer of vorticity from either side of the cylinder, rapid agglomeration of the vorticity into a large-scale Kármán-type vortex does not occur. When this layer is severed during penetration of the free surface, however, a large-scale vortex is quickly formed.

Comparison of these mechanisms of vortex formation from the surface-piercing cylinder with that from a completely submerged cylinder shows, first of all, that the latter exhibits a severe asymmetry relative to the former. Despite this asymmetry, however, there is an important common feature, namely the existence of a counter-flow mixing layer during the initial stages of separation from the cylinder and thereby an initially elongated, distributed region of vorticity, prior to agglomeration into a larger-scale concentration of vortex. For the case of the completely submerged cylinder, this process occurs from only one side of the cylinder, in contrast to the two-sided, asymmetrical formation from the surface-piercing cylinder.

REFERENCES

BEARMAN, P. W., DOWNIE, M. J., GRAHAM, J. M. R. & OBASAJU, E. D. 1985 Forces on cylinders in viscous oscillatory flow at low Keulegan-Carpenter numbers. *Journal of Fluid Mechanics* **154,** 337–356.

DOLIGALSKI, T. L., SMITH, C. R. & WALKER, J. D. A. 1994 Vortex interactions with walls. *Annual Review of Fluid Mechanics* **26,** 573–616.

IWAGAKI, Y. ASANO, T. & NAGAI, F. 1983 Hydrodynamic forces on a circular cylinder placed in

wave-current, co-existing fields. Memorandum, Faculty of Engineering, Kyoto University, Japan **45,** 11–23.

MAULL, D. J. & MILLINER, M. C. 1978 Sinusoidal flow past a circular cylinder. *Coastal Engineering* **2,** 149–168.

OBASAJU, E. D., BEARMAN, P. W. & GRAHAM, J. M. R. 1988 A study of forces, circulation and vortex patterns around a circular cylinder in oscillating flow. *Journal of Fluid Mechanics* **196,** 467–494.

ROCKWELL, D., MAGNESS, C., TOWFIGHI, J., AKIN, O. & CORCORAN, T. 1993 High-image-density particle image velocimetry using laser scanning techniques, *Experiments in Fluids* **14,** 181–192.

SARPKAYA, T. & ISAACSON, M. 1981 *Mechanics of Wave Forces on Off-Shore Structures.* New York: Van Nostrand Reinhold Company.

SINGH, S. 1979 Forces on bodies in an oscillatory flow. Ph.D. Thesis, University of London; London, U.K.

WALKER, J. D. A. 1978 The boundary layer due to rectilinear vortex. *Proceedings of the Royal Society of London A* **359,** 167–188.

WILLIAMSON, C. H. K. 1985 Sinusoidal flow relative to circular cylinders. *Journal of Fluid Mechanics* **155,** 141–174.
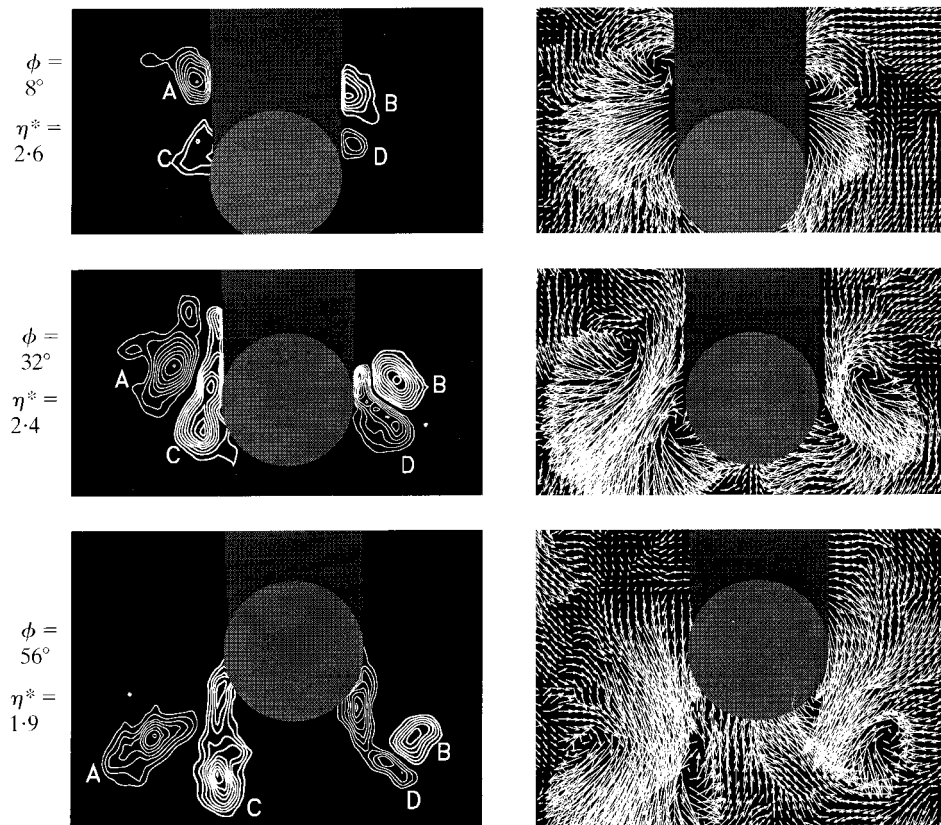
Figure 2(a). Initial phase of development of vortices from cylinder moving from its extreme position (maximum submergence) at $\eta^* = \eta/D = 2 \cdot 63$ towards the free-surface at $\eta^* = 0$. Phase angle $\phi = 0°$ corresponds to maximum submergence of cylinder. Equilibrium position of cylinder is at $h^* = h/D = 1 \cdot 1$, and amplitude of cylinder motion is $A^* = A/D = 1 \cdot 6$. Minimum and incremental values of vorticity are respectively $|\omega_{\min}| = 8 \, \text{s}^{-1}$ and $\Delta\omega = 5 \, \text{s}^{-1}$ for these and all subsequent images.
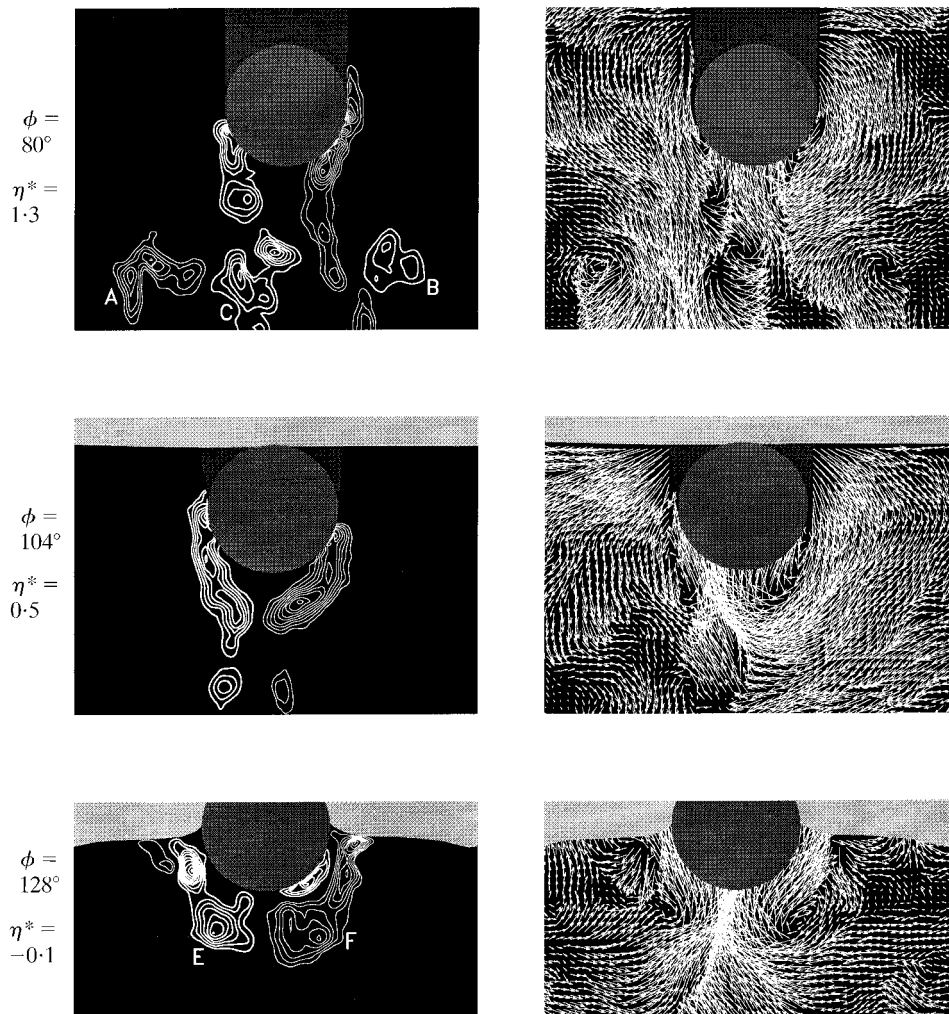
Figure 2(b). Intermediate phase of development of vortices initiated in Figure 2(a). Cylinder moves from its maximum depth of submergence at $\eta^* = 2\cdot63$ towards the free-surface at $\eta^* = 0$. Phase angle $\phi = 0°$ corresponds to maximum submergence of cylinder. Equilibrium position of cylinder is at $h^* = 1\cdot1$.

$\phi = 152°$

$\phi = 176°$

$\phi = 224°$
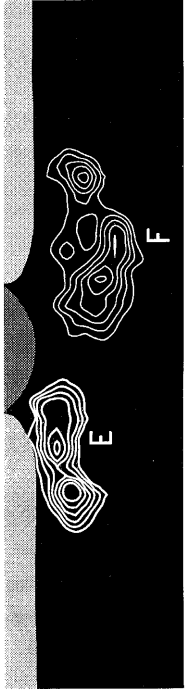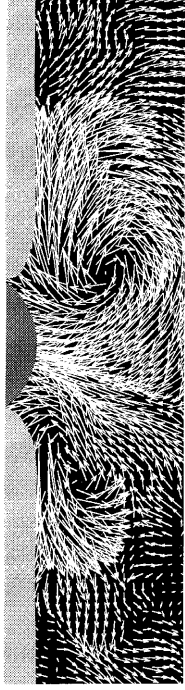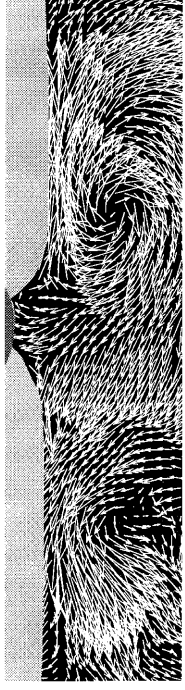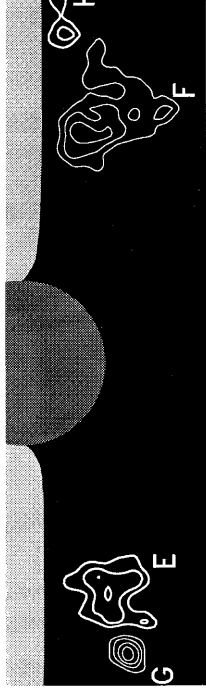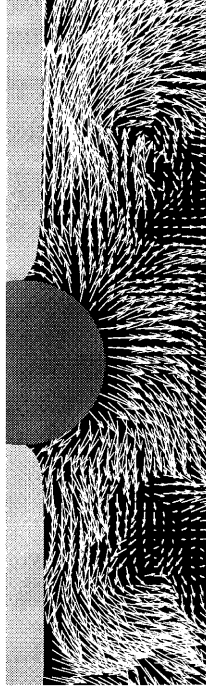
rbed free surface, then
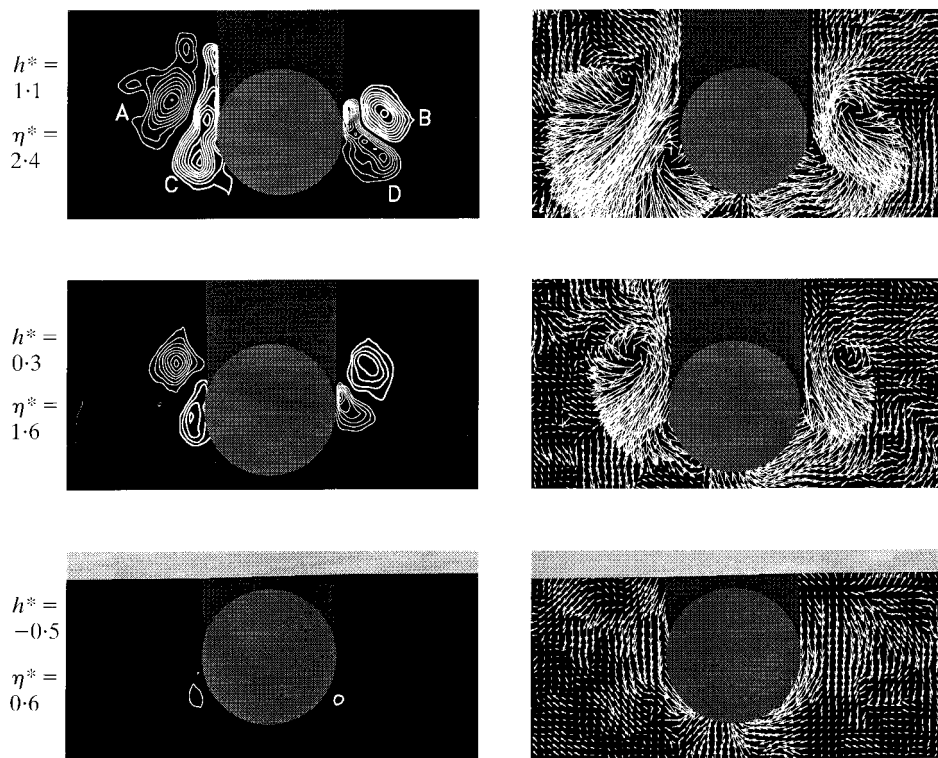
$$\phi = 32°$$

Figure 3(a). Comparison of vortex formation at same phase angle $\phi = 32°$ of cylinder motion measured from maximum depth of submergence. Depths $h^* = h/D$ of equilibrium position of cylinder are different, but amplitude $A^* = A/D = 1·6$ of cylinder motion is maintained constant.

$h^* = 1\cdot1$

$\eta^* = 1\cdot9$

$h^* = 0\cdot3$

$\eta^* = 1\cdot1$

$h^* = -0\cdot5$

$\eta^* = 0\cdot2$
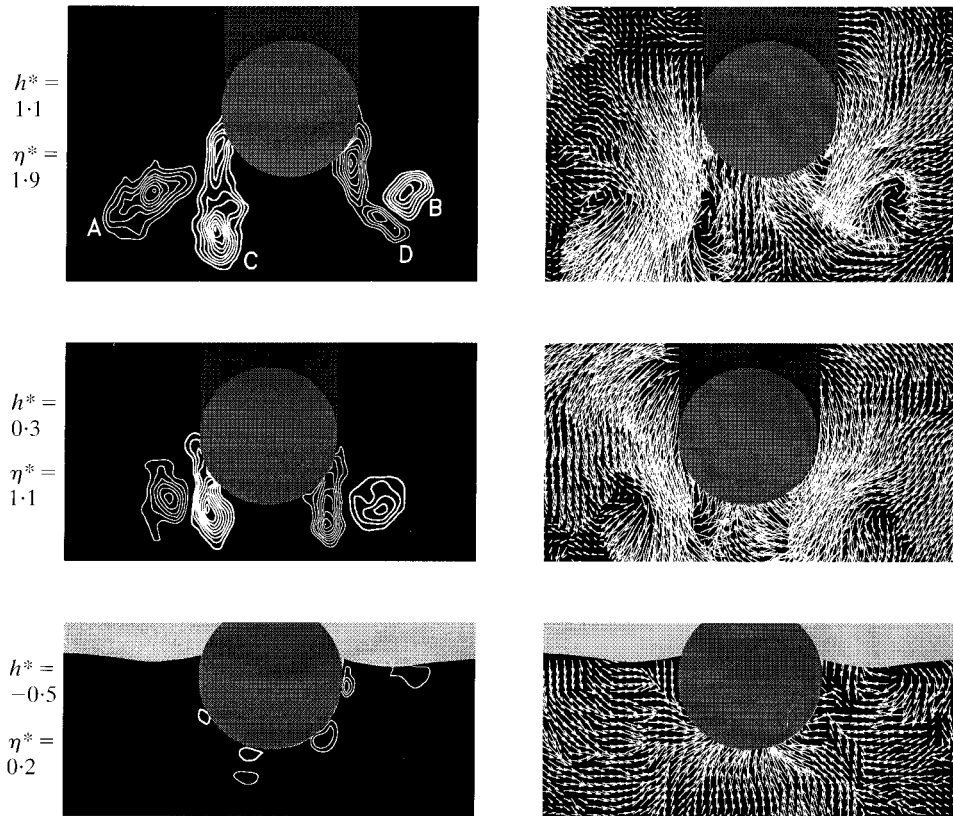
$\phi = 56°$

Figure 3(b). Same as Figure 3(a), except phase angle $\phi = 56°$.

$h^* = 1\cdot1$

$\eta^* = 1\cdot3$

$h^* = 0\cdot3$

$\eta^* = 0\cdot4$

$h^* = -0\cdot5$

$\eta^* = -0\cdot4$

A   C   B
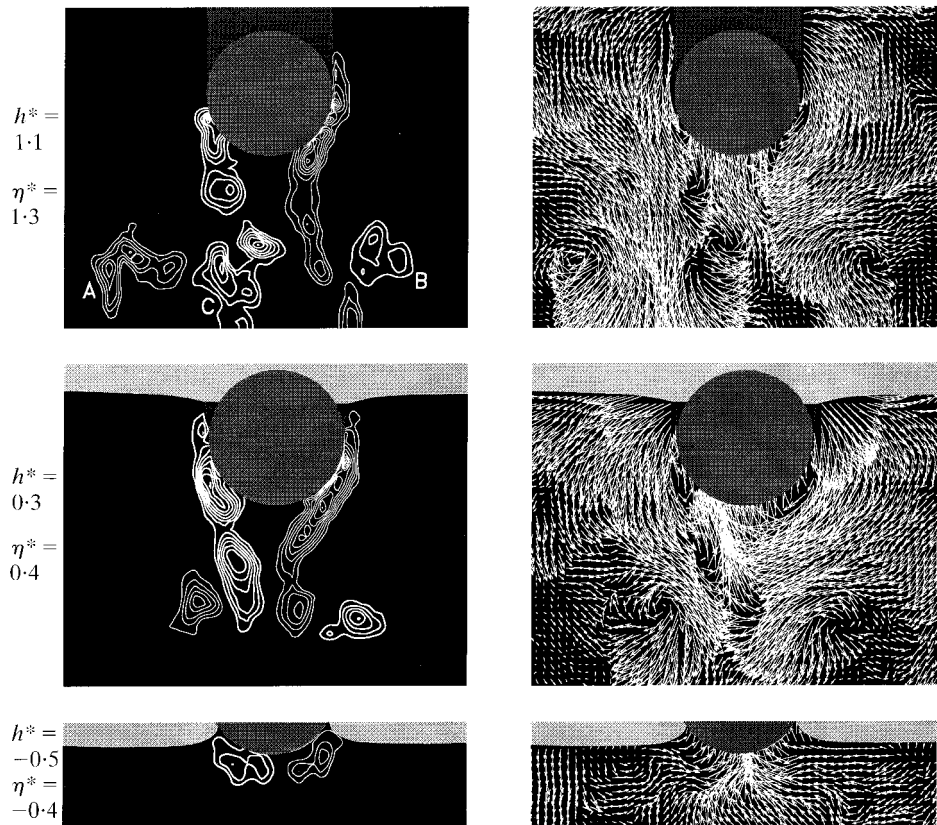
$\phi = 80°$

Figure 3(c). Same as Figure 3(a), except phase angle $\phi = 80°$.
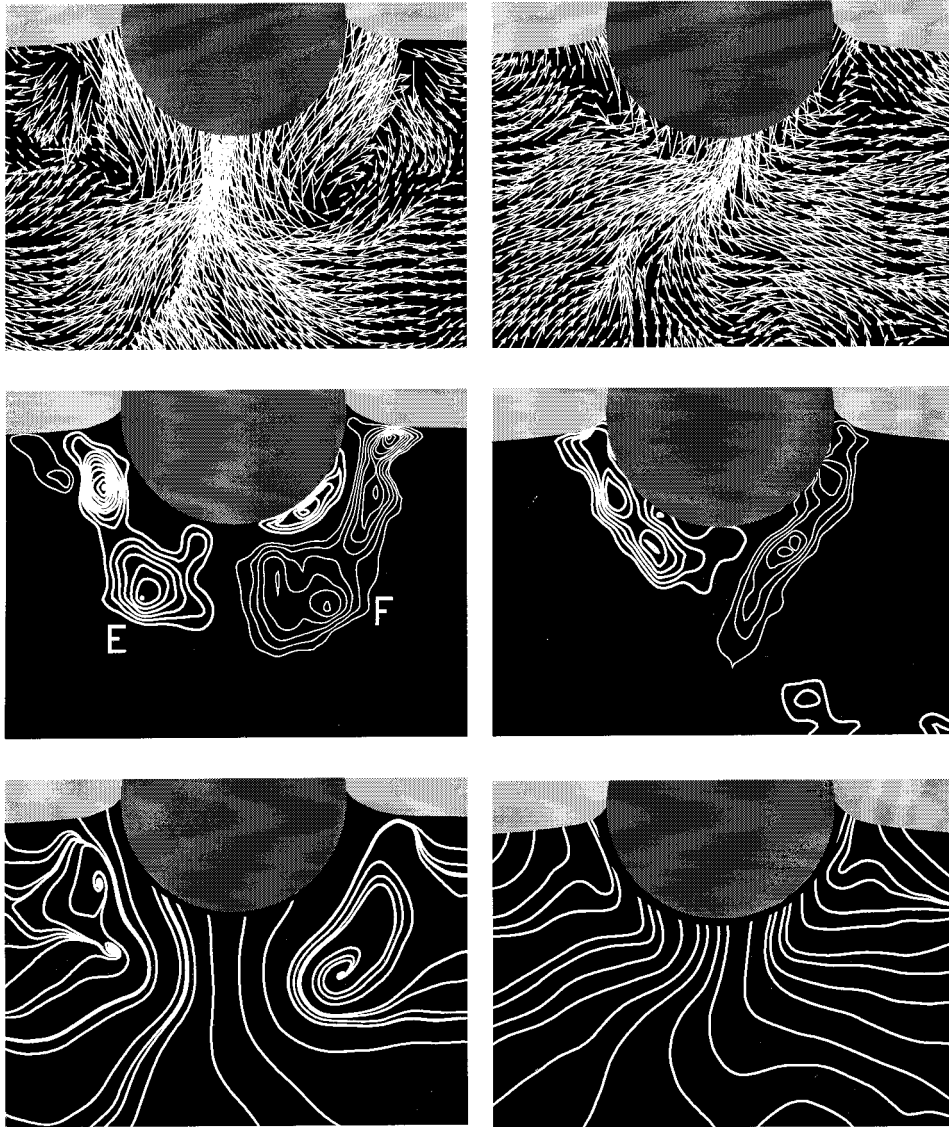
$$h^* = 1{\cdot}1, \ \phi = 128°$$ $$h^* = -0{\cdot}1, \ \phi = 80°$$

Figure 4(a). Comparison of velocity and vorticity distributions and streamline patterns for cylinder at same instantaneous position relative to the free surface, but for different equilibrium positions $h^* = h/D$ and phase angle ϕ of cylinder motion.
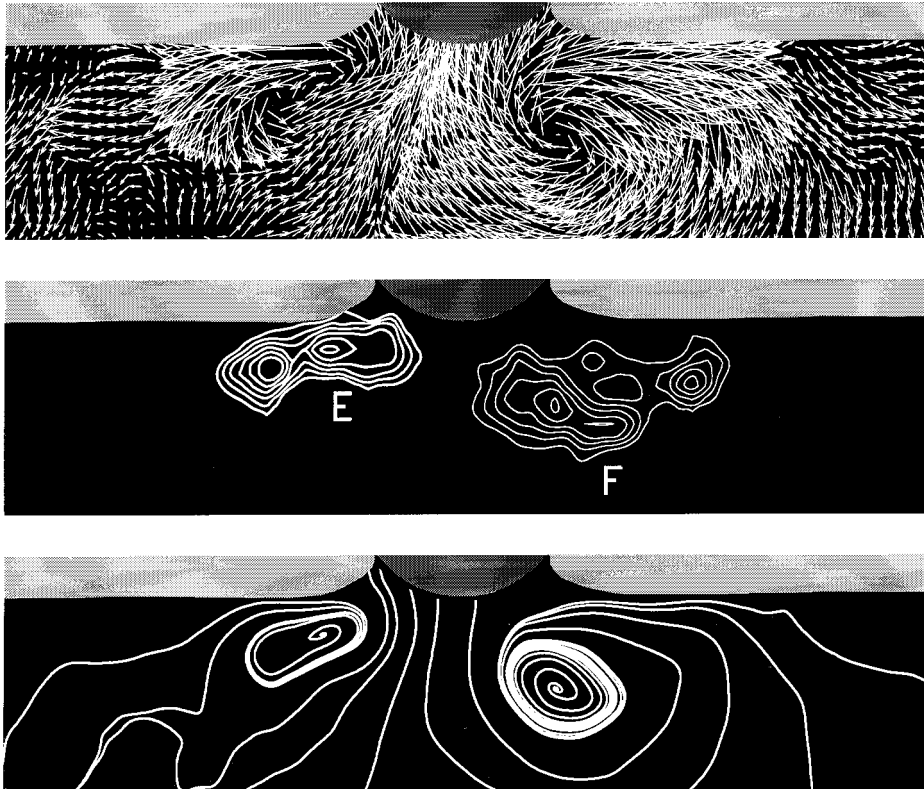
$$h^* = 1 \cdot 1, \ \phi = 152°$$

Figure 4(b). Continuation of vortex development shown in left column of Figure 4(a). The above images correspond to instant immediately following detachment of vorticity concentrations from the cylinder. Equilibrium position of cylinder is $h^* = h/D$. Phase angle of ϕ of cylinder motion is measured relative to $\phi = 0°$ corresponding to maximum depth of submergence.
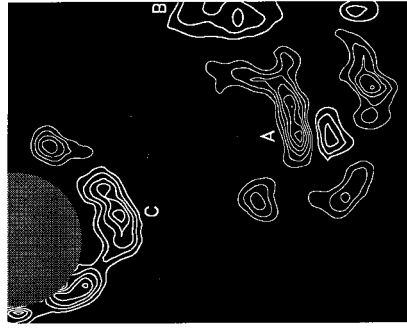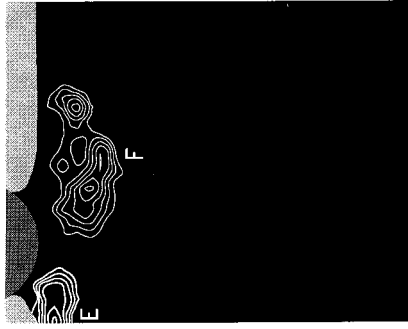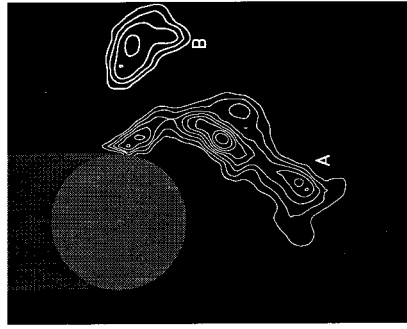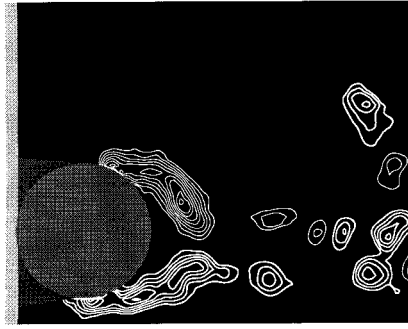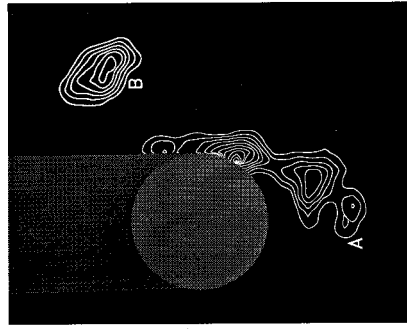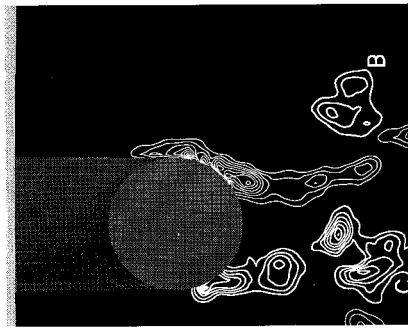
Surface
piercing

Completely
submerged

$\phi = 80°$ $\phi = 104°$ $\phi = 152°$

ged (bottom row). For both
num depth of submergence.
$i* = h/D = 1·1$ beneath free

$\phi = 80°$　　$\phi = 104°$　　$\phi = 152°$

n in Figure 5(a).

Surface piercing
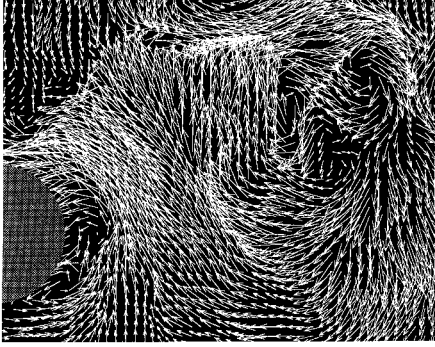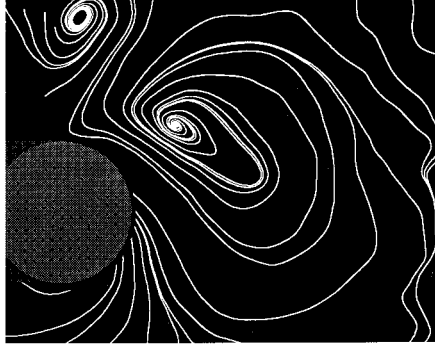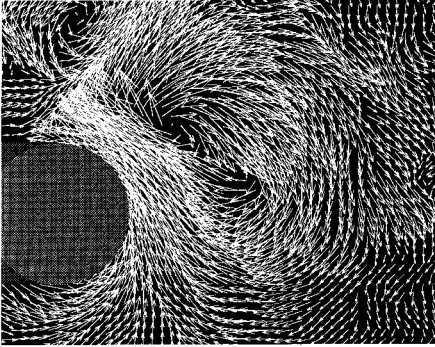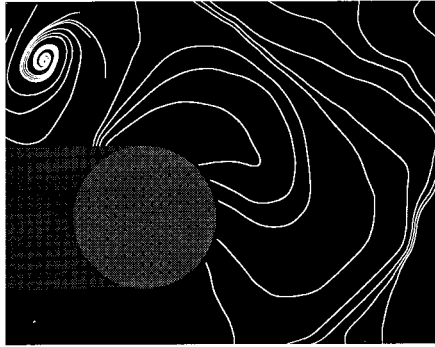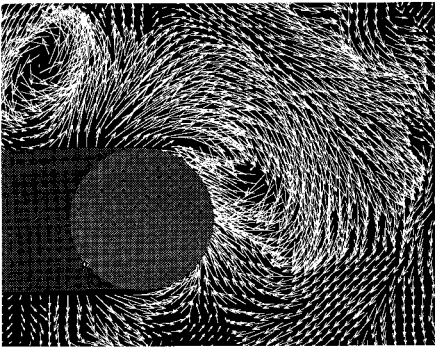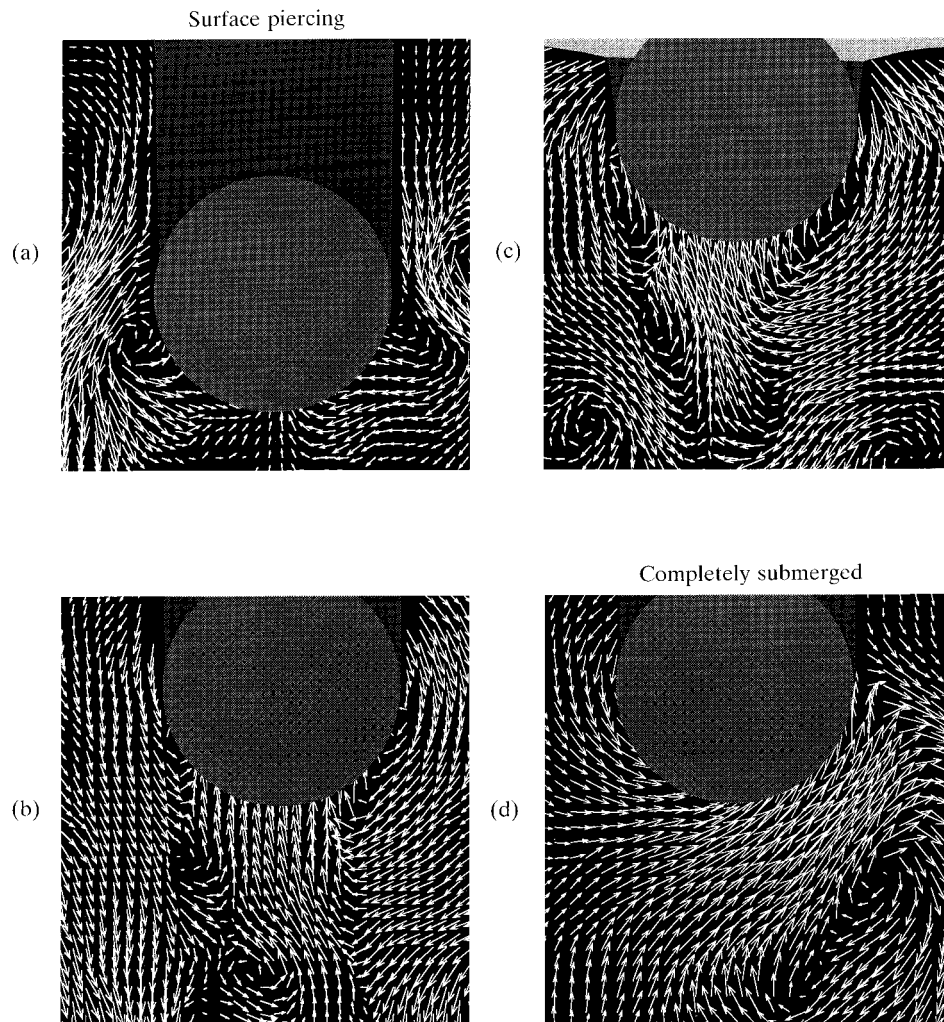
Figure 6. Close-ups of instantaneous velocity fields associated with basic classes of vorticity layer development and vortex formation. In all cases, amplitude $A^* = A/D = 1.6$ and dimensionless frequency $fD^2/v = 227$ are maintained constant. (a) equilibrium position $h^* = h/D = 1.1$ and phase angle $\phi = 32°$; (b) $h^* = 1.1$ and $\phi = 80°$; (c) $h^* = 0.3$ and $\phi = 80°$; (d) for completely submerged cylinder, $\phi = 104°$.